ELSEVIER

Ultramicroscopy 75 (1998) 53–60

ultramicroscopy

A spherical-aberration-corrected 200 kV transmission electron microscope

Max. Haider[a,*,1], Harald Rose[b], Stephan Uhlemann[a,1], Eugen Schwan[a,1], Bernd Kabius[c], Knut Urban[c]

[a] *European Molecular Biology Laboratory, Postfach 102209, D-69012 Heidelberg, Germany*
[b] *Institut für Angewandte Physik, Technische Hochschule Darmstadt, D-64289 Darmstadt, Germany*
[c] *Institut für Festkörperforschung, Forschungszentrum Jülich GmbH, D-52425 Jülich, Germany*

Received 21 March 1998; received in revised form 5 June 1998

Abstract

A hexapole corrector system was constructed for compensation of the spherical aberration of the objective lens of a transmission electron microscope. Implementing this system on a commercial 200 kV instrument with a field emission gun the spherical aberration correction was demonstrated and an improvement of the point resolution from 0.24 nm to better than 0.14 nm was realized. Applying the new instrument to structure studies on $Si/CoSi_2$ interfaces it was demonstrated that an outstanding additional advantage of aberration correction is the substantially reduced contrast delocalization in high-resolution images.

PACS: 61.16.Bg; 41.90. + e

Keywords: Transmission electron microscopy; Spherical aberration; Spherical-aberration correction; Structure images; Contrast delocalization

1. Introduction

The reduction of lens aberrations poses a fundamental problem of optical design. Only by correcting aberrations does it become possible to push the deviations from ideal Gaussian optics [1] to values below certain tolerance limits. Since the invention of the transmission electron microscope (TEM) by Knoll and Ruska [2] in 1932, the aberrations of electron lenses have been studied intensively [3]. Fifty years ago, Scherzer [4] suggested that the two major axial aberrations, chromatic and spherical aberration, could be corrected by a combination of electromagnetic quadrupole and octupole elements. Unfortunately, the realization of this suggestion proved to be difficult although it was shown by Koops et al. [5] and Hely [6] that a multipole

* Corresponding author.
[1] Now at CEOS GmbH, Im Neuenheimer Feld 519, D-69120 Heidelberg, Germany. E-mail: haider.ceas@t-online.de.

0304-3991/98/$ – see front matter
PII: S0304-3991(98)00048-5

corrector, based on calculations by Rose [7], functions in principle. However, the technical problems were too complex to be tackled by the means available at the time, and even today the point resolution in transmission electron microscopy is limited by the spherical aberration of the objective lens. On the other hand Zach and Haider [8] recently succeeded in developing a corrector system for a low-voltage scanning electron microscope where the conditions for aberration correction are more favourable. They were thus able to improve the resolution of the probe-forming system from 5 nm to below 2 nm at an electron energy of 1 keV.

Till date, in transmission electron microscopy, the only way to improve the resolution consisted of a numerical correction of spherical aberration effects a posteriori on the basis of a series of images of the object taken under variable objective-focus conditions [9–11] and by the application of holographic techniques [12]. We have now succeeded in constructing a hexapole corrector system to compensate the spherical aberration of the objective lens of a 200 kV transmission electron microscope. Implementing this system on a Philips CM 200 with a field-emission gun (FEG) we were able to demonstrate the spherical aberration correction and to realize an improvement of the point resolution from 0.24 nm to better than 0.14 nm. In addition, by a first application of this microscope to the study of the atomic structure of $Si/CoSi_2$ interfaces, we were able to demonstrate a substantial reduction in contrast delocalization, a phenomenon which has till date severely hampered the use of transmission electron microscopes equipped with field emission sources in structure studies on atomic dimensions. In this paper we present a brief report on how aberration correction was achieved and on the first results obtained in the application of the new instrument.

2. Correction of spherical aberration

Our electron-optical solution for spherical aberration correction follows a suggestion by Rose [13]. It is based on two electromagnetic hexapoles and four additional lenses [14]. The principle by which correction is achieved is based on the fact that the *primary* non-rotationally symmetric second-order aberrations of the first hexapole are compensated by the second hexapole element. Owing to their non-linear diffraction power, the two hexapoles additionally induce a residual *secondary* third-order spherical aberration which is rotationally symmetric [15] and proportional to the square of the hexapole strength. The sign of the appertaining coefficient of spherical aberration is opposite to that of the objective lens. Accordingly, the spherical aberration of the entire system can be eliminated by exciting the hexapoles appropriately. And hence, such a hexapole corrector was first proposed for a scanning transmission electron microscope for which off-axial aberrations have not do be taken into account [16,17].

In the TEM off-axial aberrations are as important as axial ones. Therefore, in order to maintain a sufficiently large field of view, an aplanatic or a semi-aplanatic objective lens system (Fig. 1) has to be employed which fulfils the Abbe sine condition. This implies that it is not only free of spherical aberration but also of off-axial coma and of parasitic axial aberrations resulting from misalignments of the optical system. In order to eliminate the

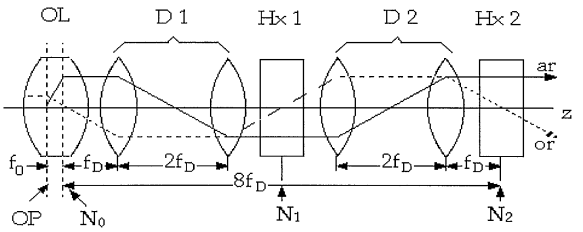

Fig. 1. The new semi-aplanatic objective lens system consists of a compound lens OL (f_0 denotes the focal length of the objective lens), two transfer round-lens doublets (D1 and D2) of focal length f_D, and two hexapoles (Hx1 and Hx2). OP is the object plane and N_0, N_1, and N_2 denote the position of the outer nodal planes of the doublets. These are also the coma-free planes. Every possible ray is a linear combination of the two principal rays the axial ar and off-axial ray or. In order to compensate the primary aberrations of the hexapoles Hx1 is imaged into Hx2 with unit magnification by centring the hexapoles at N_1 and N_2. The total third-order spherical aberration of the imaging system (objective-lens, transfer-lenses and projector system) is corrected by the residual negative secondary aberration of the hexapoles.

radial (isotropic) component of the off-axial coma the coma-free plane of the objective lens has to be matched with the coma-free plane of the corrector. This is achieved by means of the transfer-lens doublet D1. For reduction of the azimuthal (anisotropic) component of the off-axial coma the current direction of the first transfer-lens doublet D1 is opposite to that in the objective lens. Thus, the off-axial coma is minimized to a value which allows high-resolution imaging of an object area sufficiently large for any practical application. In our system, the field of view has a diameter of at least 100 nm corresponding to 2000 pixels per diameter if the Nyquist frequency is taken as $10\,\mathrm{nm}^{-1}$.

The second-order aberrations of the hexapoles cancel out if the first hexapole is imaged onto the second with negative unit magnification. The spherical aberration of the system is then compensated by the residual negative third-order spherical aberration of the hexapoles. After correction of the third-order spherical aberration, a fifth-order spherical aberration remains. It consists of a rotationally symmetric part with coefficient C_5, and a part with sixfold symmetry. The latter can be compensated by a duodecapole if necessary. In our case, the measured fifth-order aberrations were negligibly small within an aperture of spatial frequency $q = 7\,\mathrm{nm}^{-1}$ [18].

The incorporation of the corrector itself does not suffice to improve the resolution of the microscope. A reliable alignment procedure is an essential additional pre-requisite. In fact, it is mandatory to additionally compensate the parasitic second-order axial aberrations, coma and threefold astigmatism, and to adequately suppress the non-spherical axial third-order aberrations, star aberration and fourfold astigmatism. For this purpose, in the new instrument, the aberration coefficients are determined by means of an extended version of the diffractogram-tableau method proposed by Zemlin et al. [19,18]. With the corrector switched off, diffractograms of an amorphous sample are recorded digitally and evaluated on-line in terms of defocus and twofold astigmatism induced by tilting the illumination. Subsequently, the currents required for compensation of the aberrations are calculated and applied to the coils of specially designed stigmators. The subsequent excitation of the corrector elements introduces additional misalignment aberrations and the procedure has to be repeated.

3. The spherical aberration-corrected electron microscope

The basic instrument used for this development was a standard 200 kV Philips CM 200 FEG ST equipped with a field emission gun (FEG). The objective lens had a focal length of $f_0 = 1.7$ mm, a coefficient of spherical aberration of $C_s = 1.23$ mm and a coefficient of chromatic aberration of $C_c = 1.3$ mm. The corrector increases the column height by 24 cm but leaves the other operating modes and functions of the microscope unaffected, including the option for STEM operation and X-ray analysis.

The computer-assisted semi-automatic alignment of the instrument takes about 15 min on a daily routine basis. The aligned state lasts for typically 1–2 h, after which a brief fine tuning may be necessary. The Zemlin tableau of the uncorrected microscope is shown in Fig. 2a and that of the corrected and properly aligned system in Fig. 2b. All the diffractograms in Fig. 2b exhibit about the same shape demonstrating the properties of an aplanatic objective lens. Even for beam tilt angles as high as 30 mrad the values of defocus and twofold astigmatism induced by the residual axial aberrations remain small. The wave phase shift due to residual aberrations is less than $\pi/4$ up to spatial frequencies of $q = 7\,\mathrm{nm}^{-1}$.

Fig. 3 demonstrates the resolution of the corrected microscope by means of the Young fringes technique [20] applied to a thin amorphous tungsten film using the standard Philips single-tilt side-entry specimen holder. We find a resolution limit of 0.12 nm in the direction of the long axis of the goniometer and 0.14 nm perpendicular to it.

4. The phase-contrast transfer function

Since high-resolution electron microscopy is, in general, carried out under phase-contrast conditions it appears appropriate to briefly discuss the effect of spherical-aberration compensation on the

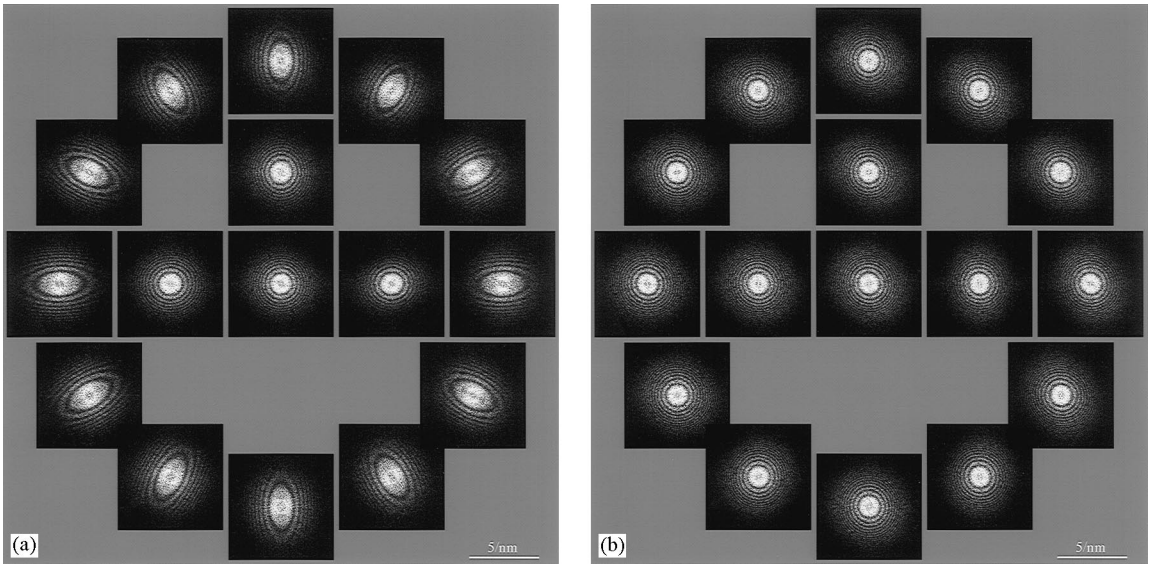

Fig. 2. Diffractogram tableaus of (a) the uncorrected microscope and (b) after spherical-aberration correction and proper alignment. The beam tilt angle is 10.8 mrad in both cases and the azimuthal angles vary between 0 to 2π in steps of $\pi/6$. The essentially identical shape of the diffractograms in (b) indicates aplanatic properties.

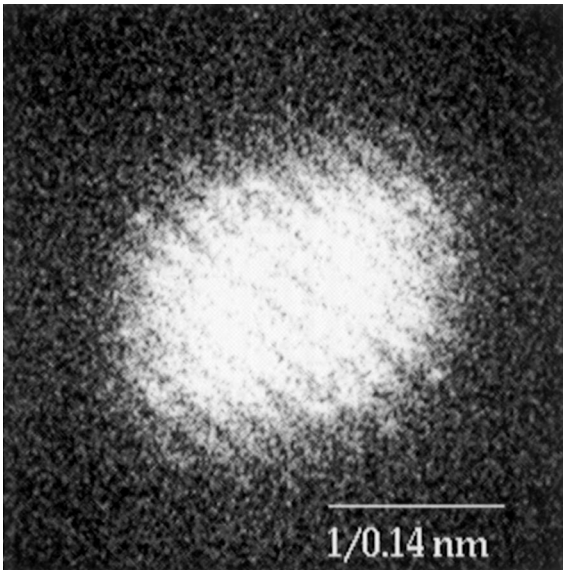

Fig. 3. Experimental Young fringes test of the information limit on an amorphous tungsten thin-film specimen. The information limit of the aberration-corrected microscope is 0.12 nm in the direction of the long axis of the single-tilt specimen holder and 1.4 nm in the direction perpendicular to it.

phase-contrast transfer function. A detailed account is given in a separate paper [21].

The phase-contrast transfer function (PCTF) gives the contrast expressed by the sine of the phase angle at which, at a certain deviation Δf from the Gaussian focus f_0, a given space frequency q contributes to the image of a thin phase object [22]. The PCTF calculated for the basic instrument, under Scherzer defocus conditions at 200 kV, i.e. for an underfocus of $\Delta f = 68$ nm, is displayed in Fig. 4 (dashed line). Defining the *point resolution* as the inverse of the maximum space frequency up to which the waves contribute to the image with contrast of the same sign yields 0.24 nm for the uncorrected TEM. The damping of the PCTF at high q is caused by chromatic aberration, limited temporal and spatial coherence and by mechanical and electrical instabilities [22]. The resulting damping envelope determines the *information limit* which, taking into account only chromatic and spherical aberration, is about 0.12 nm.

The corresponding PCTF calculated for the aberration-corrected microscope is displayed in Fig. 4 (solid line). Since, in structure imaging, we have to convert phase shifts into an intensity variation, the

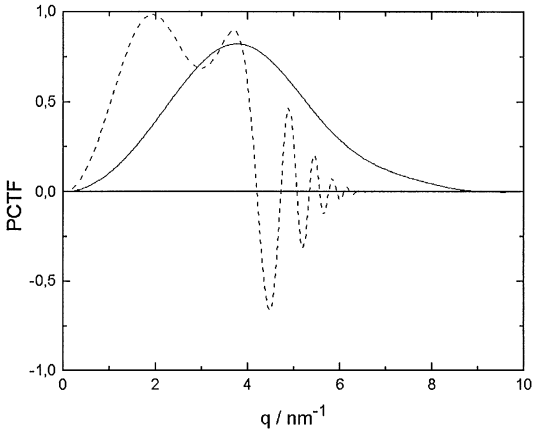

Fig. 4. Calculated phase contrast transfer function for the uncorrected (dashed line, $C_s = 1.23$ mm, $\Delta f = 68$ nm, $C_c = 1.3$ mm) and the corrected (solid line, $C_s = 0.05$ mm, $\Delta f = 14$ nm, $C_c = 1.7$ mm) microscope. q denotes the space frequency. In the case of the aberration-corrected microscope the point resolution essentially coincides with the information limit. Both curves were calculated for the respective Scherzer defocus. The damping envelope was calculated assuming $\Delta E = 0.7$ eV (FWHM) for the energy width and 0.2 mrad for the semi-convergence angle in both cases.

corrector has to be adjusted to maintain a certain appropriately chosen C_s value. This was chosen to be 0.05 mm. With a measured width of the electron energy distribution of the microscope of 0.7 eV (FWHM) the PCTF drops to a value of about 0.1 at $q \approx 7.5\ \mathrm{nm}^{-1}$. No contrast oscillations occur at the Scherzer defocus of $\Delta f = 14$ nm belonging to the adjusted C_s value. The point resolution is improved up to a value close to the information limit, i.e., to about 0.14 nm. The low contrast of the corrected TEM for low spatial frequencies is caused by the relatively small value of the Scherzer defocus. In calculating the damping envelope of the PCTF it was taken into account that the introduction of the transfer lenses increases the coefficient of the chromatic aberration of the entire system consisting of objective lens and corrector by about 30% to $C_c = 1.7$ mm. However, it is important to point out that the overall damping of the PCTF, at Scherzer defocus, is still smaller than that of the uncorrected microscope due to the strongly reduced influence of the spatial incoherence on the damping of the PCTF achieved by the spherical aberration correction.

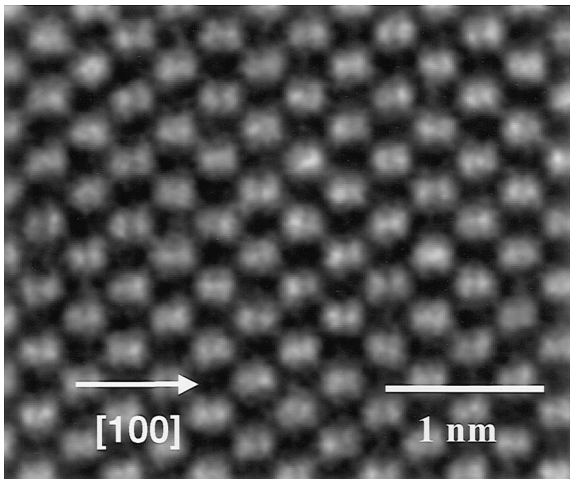

Fig. 5. Structure image of a GaAs crystal viewed along a $\langle 1\,1\,0\rangle$-direction. The crystal was oriented by means of a standard Philips $\pm 40^\circ$ double-tilt holder. The atom positions appear light on a dark background.

5. Structure imaging in the spherical-aberration-corrected microscope

Fig. 5 shows a GaAs crystal imaged along a $\langle 1\,1\,0\rangle$ – lattice direction which was adjusted by means of the standard Philips $\pm 40^\circ$ double-tilt sample holder. The image was taken with the corrected microscope, and the dumb-bell-shaped pairs of Ga and As atoms with a spacing of 0.14 nm are well resolved. Up to now such *direct* structure imaging of GaAs in $\langle 1\,1\,0\rangle$ orientation, at Scherzer defocus, has only been possible at an electron energy of 1.25 MeV in a high-voltage electron microscope where additional efforts were undertaken to achieve an especially low width of the electron energy distribution [23]. In this microscope, the resolution is sufficiently high due to the reduced electron wavelength.

A unique advantage of spherical-aberration correction is that structure-imaging artefacts due to contrast delocalization can be avoided to a great extent. These artefacts have turned out to be a major obstacle for the application of FEG instruments to defect and interface studies [24]. Contrast delocalization arises from the width of the point spread function, i.e. the width of the aberration discs belonging to the individual diffracted electron waves whose diameter increases with C_s. The resulting

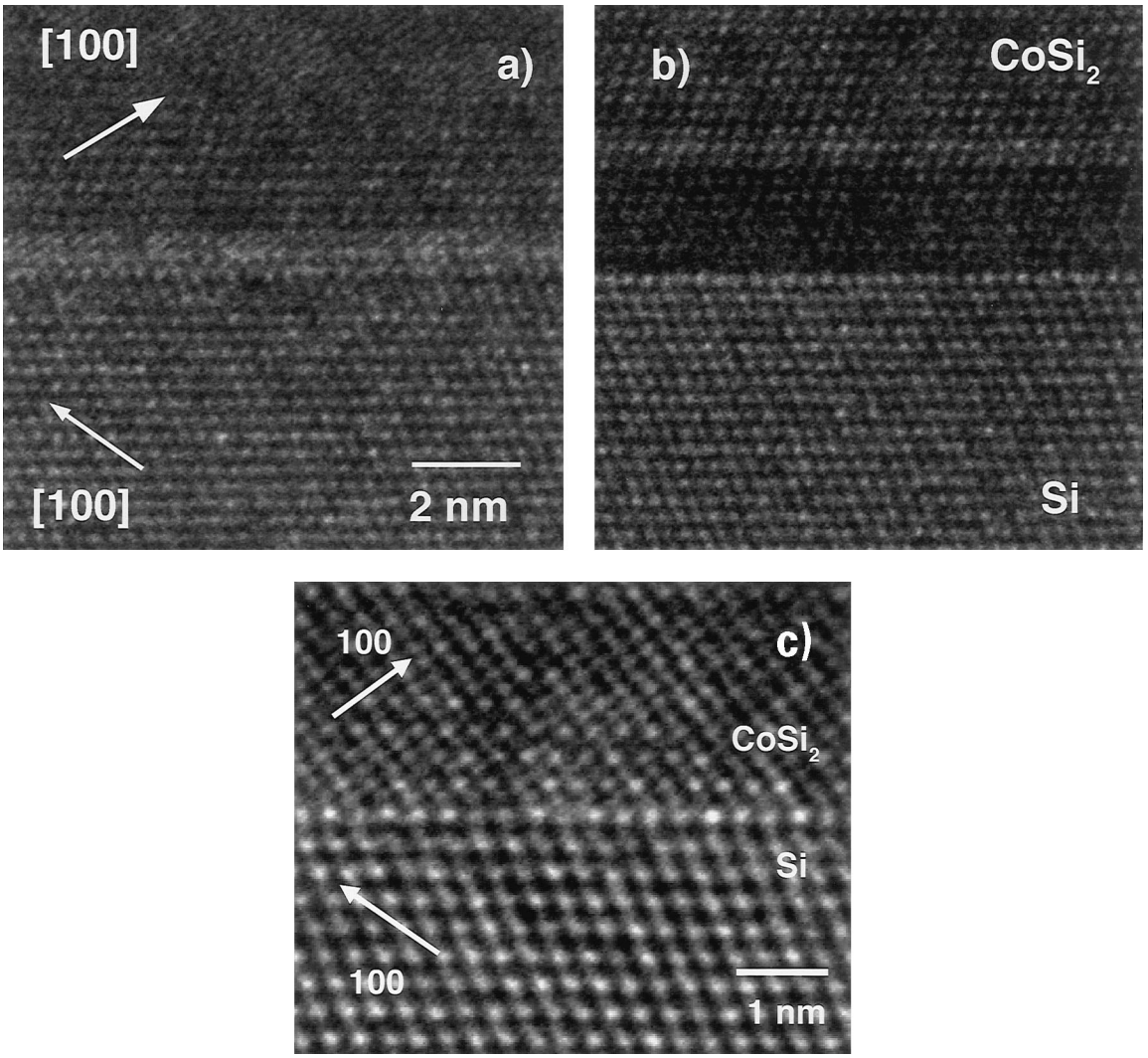

Fig. 6. Structure images of an epitaxial Si(1 1 1)/$CoSi_2$ interface demonstrating the production of image artefacts by the effect of contrast delocalization due to spherical aberration. Images (a) and (b) were taken in the uncorrected microscope at Scherzer defocus and defocus of least confusion, respectively. Image (c), taken in the aberration-corrected microscope at Scherzer defocus, does not show any contrast delocalization ($C_s = 0.05$ mm).

artefacts are especially pronounced in the region of non-periodic structures because in this case the random overlap of waves scattered at different atoms cause speckles in the image. Fig. 6a shows, in a cross-sectional preparation, the interface of $CoSi_2$ grown epitaxially on Si(1 1 1) seen along $\langle 1\,1\,0 \rangle$. The image was taken under Scherzer defocus conditions without correction. At the interface an approximately 2 nm broad region of darker contrast can be seen. The width depends on the defocus value reaching a minimum at the focus of least confusion (Fig. 6b). However, even under these conditions the width of the interface region influenced by delocalization comprises about three atomic monolayers. If the structure is imaged with the aberration-corrected objective lens (Fig. 6c) the delocalization has essentially disappeared and the interface appears atomically sharp.

6. Discussion

We have been able to demonstrate for the first time that spherical-aberration correction is applicable in high-resolution transmission electron microscopy. This opens up entirely new possibilities of improving the resolution without the need to use very high electron energies or to reduce the spherical aberration of objective lenses by a further reduction of the geometrical pole-piece dimensions. The 200 kV spherical-aberration-corrected microscope avoids the radiation damage produced in the samples by atomic knock-on processes at higher accelerating voltages. In addition the possibility of using the standard pole pieces means that the ranges for specimen translation and tilt as well as the installation and use of equipment for X-ray spectroscopy are not affected.

The potential of spherical-aberration-corrected transmission electron microscopes for materials research has still to be investigated in detail. The absence or at least, depending on the C_s value adjusted, strong reduction of contrast delocalization is of great benefit for quantitative defect and interface studies. We also would like to point out the advantages in connection with the application of the image calculation techniques. Indeed, images of the type of Fig. 6 contain a substantial amount of quantitative information which is, however, encoded by the quantum mechanics of the passage of the electrons through the specimen. Quantum-mechanical image calculations and numerical wave-function retrieval techniques are therefore part of current electron-microscopic practice [10,11,25–27]. The aberration-corrected microscope, with its oscillation-free PCTF, greatly facilitates this quantitative image interpretation and, in addition, since very large beam-tilt angles are available, makes it easier to measure the imaging parameters. This is also an advantage for the application of holographic techniques.

We have not yet been able to explore the consequences of spherical aberration correction for Bragg diffraction contrast imaging employed in the study of extended objects, e.g. grain boundaries and dislocations. We expect advantages for tilted-beam techniques, since tilting the incident beam by up to 30 mrad does hardly affect the diffractogramm as can be seen from Fig. 2b. Furthermore, spherical aberration correction reduces the delocalization of diffraction information which, in conventional electron microscopes, limits local structure analysis by selected area diffraction to regions larger than about 1 μm in diameter.

There are indications that, with respect to resolution, the theoretical limits of our aberration-corrected microscope have not yet been reached. The observation that the resolution measured by the Young fringes test is different in the direction parallel to the long axis of the side-entry specimen holder from that obtained in the perpendicular direction points to mechanical instabilities of the stage. This is only an additional indication of the fact that approaching the ultimate resolution of the instrument requires a joint optimization of all components. Further technical developments are in progress. We note that a significant further increase of the resolution into the sub-ångström range requires a lowering of the electron-energy spread of the source or an additional corrector system for the chromatic aberration of the objective lens.

Acknowledgements

We thank the Volkswagen-Stiftung for funding this project. Its realization would not have been possible without the support of L. Philipson, former Director-General of EMBL, and of J. Treusch, Chairman of the Board of Research Centre Jülich. Thanks are due to the members of the workshops at EMBL and to H. Wittman for technical assistance and to J. Zach for innumerable helpful discussions. We are also grateful, in particular to K. van der Mast, for the support provided by Philips Electron Optics. The $Si/CoSi_2$ samples were generously provided by S. Mantl, F. Klinkhammer and St. Meesters.

References

[1] M. Born, E. Wolf, Principles of Optics, Pergamon Press, Oxford, 1980.
[2] M. Knoll, E. Ruska, Z. Physik 78 (1932) 318.
[3] O. Scherzer, Z. Physik 101 (1936) 593.
[4] O. Scherzer, Optik 2 (1947) 114.

[5] H. Koops, G. Kuck, O. Scherzer, Optik 48 (1977) 225.
[6] H. Hely, Optik 60 (1982) 353.
[7] H. Rose, Optik 34 (1971) 285.
[8] J. Zach, M. Haider, Nucl. Instr. and Meth (1995) 316.
[9] E.J. Kirkland, Ultramicroscopy 15 (1984) 151.
[10] A. Thust, M.H.F. Overwijk, W.M.J. Coene, M. Lentzen, Ultramicroscopy 64 (1996) 249.
[11] W.M.J. Coene, A. Thust, M. Op de Beeck, D. Van Dyck, Ultramicroscopy 64 (1996) 109.
[12] H. Lichte, Ultramicroscopy 20 (1986) 293.
[13] H. Rose, Optick 85 (1990) 19.
[14] M. Haider, G. Braunshausen, E. Schwan, Optick 99 (1995) 167.
[15] V.D. Beck, Optick 53 (1979) 241.
[16] H. Rose, Nucl. Instr. and Meth. 187 (1981).
[17] A.V. Crewe, Optik 55 (1982) 271.
[18] S. Uhlemann, M. Haider, Ultramicroscopy 72 (1998) 109.
[19] F. Zemlin, K. Weiss, P. Schiske, W. Kunath, K.H. Herrmann, Ultramicroscopy 3 (1977) 49.
[20] J. Frank, Optik 30 (1969) 171.
[21] A. Thust, M. Lentzen, K. Urban, to be published.
[22] L. Reimer, Transmission Electron microscopy, Springer, Berlin, 1984.
[23] F. Phillipp, R. Höschen, M. Osaki, G. Möbus, M. Rühle, Ultramicroscopy 56 (1994) 1.
[24] A. Thust, W.M.J. Coene, M. Op de Beek, D. Van Dyck, Ultramicroscopy 64 (1996) 211.
[25] J.C.H. Spence, Experimental High-Resolution Electron Microscopy, Oxford University Press, Oxford, 1998.
[26] M.A. O'Keefe, R. Kilaas, Proc. 6th Pfefferkorn Conf. On Image and Signal Processing, Scanning Microscopy Inc., Chicago, 1988, p. 225.
[27] P.A. Stadelmann, Ultramicroscopy 21 (1987) 131.